Journal of Biochemistry and Biophysics
Volume 4 | Issue 1
ISSN: 2576-7623

Research Article Open Access

In Silico Discovery of Natural Compounds as Inhibitors of the RET Signaling Pathway in Cancer

Farideh Ghalamfarsa[2,*], Azizeh ShadiDizaji[1], Kagan Tolga Cinisli[3], Mohamad Warda[4,5] and Ahmet Haci muftuoglu[1]

[*]**Corresponding Author**: Ghalamfarsa Farideh, Cellular and Molecular Research Center, Yasuj University of Medical Sciences, Yasuj, Iran, Tel: +09389790247, E-mail: farideh.ghalamfarsa@yahoo.com

Citation: Farideh Ghalamfarsa, Azizeh ShadiDizaji, Kagan Tolga Cinisli, Mohamad Warda, Ahmet Haci muftuoglu, et al. (2026) In Silico Discovery of Natural Compounds as Inhibitors of the RET Signaling Pathway in Cancer, J Biochem Biophy 4(1): 101

Received Date: January 08, 2026 **Accepted Date:** February 06, 2026 **Published Date:** February 09, 2026

Abstract

Aberrant activation of the rearranged during transfection (RET) signaling pathway contributes to tumorigenesis and therapeutic resistance across multiple cancer types, including thyroid, lung, and breast malignancies. Although selective RET tyrosine kinase inhibitors such as selpercatinib and pralsetinib have demonstrated clinical success, their long-term efficacy is limited by resistance mutations and off-target toxicities. This study employed a comprehensive in silico strategy to identify natural compounds with potential inhibitory activity against the RET kinase domain (PDB ID: 7JU6). A curated library of 48 natural molecules from the ZINC database was screened using molecular docking via AutoDock Vina, followed by pharmacokinetic and toxicity profiling with pkCSM. Four compounds, ZINC05202250, ZINC00338411, ZINC13374352, and ZINC13379108, exhibited strong binding affinities (−8.0 to −8.8 kcal/mol) and stable docking conformations within the active pocket defined by key residues VAL26A and LYS46A. Interaction analysis revealed a conserved hydrophobic network complemented by hydrogen bonds and salt bridges, indicating robust ligand anchoring within the ATP-binding cleft. ADMET predictions highlighted high intestinal absorption (>95%), low cardiotoxicity (hERG-negative), and absence of mutagenic potential (AMES-negative). Among these, ZINC05202250 and ZINC13379108 emerged as the most promising leads, combining optimal binding energies with favorable pharmacokinetic and safety profiles. Overall, this in silico pipeline identifies naturally derived RET inhibitors with strong drug-like characteristics, providing a rational foundation for further in vitro and in vivo validation toward developing safer and more selective therapeutics for RET-driven cancers.

Keywords: RET Kinase; Natural Inhibitors; Molecular Docking; Pharmacoinformatics; ADMET Profiling; Cancer Therapeutics

Introduction

Globally, cancer persists as a primary contributor to mortality, with its intricate nature arising from aberrant signaling cascades that drive aberrant cellular proliferation, viability, and dissemination of neoplastic cells [1]. Within this framework, receptor tyrosine kinases (RTKs) are instrumental in conveying extracellular cues to intracellular effectors and frequently exhibit dysregulated activation in malignant cells [2]. The RET (rearranged during transfection) proto-oncogene, encoding a transmembrane RTK essential for neoplastic cell expansion, persistence, and maturation, exemplifies this mechanism [3]. Initially discovered in the mid-1980s via transfection assays involving lymphoma DNA, RET has subsequently been associated with diverse ontogenetic mechanisms and disease states, encompassing multiple cancer types [4].

In the field of oncology, RET aberrations manifest as point mutations, gene rearrangements, amplifications, or overexpression, manifesting across various tumor histologies with varying prevalence [5]. For instance, specific point mutations like M918T and C634R predominate in medullary thyroid carcinoma (MTC), constituting up to 95% of hereditary instances linked to multiple endocrine neoplasia type 2 (MEN2), whereas fusions with partner genes such as KIF5B or CCDC6 are detected in 1–2% of non-small cell lung cancers (NSCLC) and 10–20% of papillary thyroid carcinomas (PTC) [6-8]. Outside of thyroid and pulmonary malignancies, RET alterations exhibit reduced frequencies in breast (1.2%), colorectal (0.2%), pancreatic, ovarian, prostate, and salivary gland carcinomas, frequently correlating with aggressive disease features, distant metastatic spread, and unfavorable outcomes [9]. As an illustration, in breast carcinoma, RET overexpression—present in 40–60% of cases—promotes endocrine therapy resistance via reciprocal crosstalk with estrogen receptor α (ERα), wherein GDNF-RET pathway activation leads to ERα phosphorylation at S118, stimulates PI3K/mTOR signaling, and diminishes the efficacy of anti-estrogen agents like tamoxifen or aromatase inhibitors [10]. Analogously, in NSCLC, RET fusions delineate a distinct molecular subgroup characterized by elevated propensity for brain metastases (27% at diagnosis), highlighting the imperative for therapeutic agents capable of crossing the blood-brain barrier [7, 11].

Such alterations not only amplify neoplastic cell proliferation cascades but also augment invasiveness via focal adhesion kinase (FAK) phosphorylation and facilitation of epithelial-mesenchymal transition, as evidenced in preclinical models of pulmonary and mammary metastases [12]. The therapeutic framework for RET-dependent malignancies has undergone swift progression, moving from multikinase inhibitors (MKIs) to highly selective RET tyrosine kinase inhibitors (TKIs) [13]. In recent years, targeted TKI agents including selpercatinib (LOXO-292) and pralsetinib (BLU-667) have transformed clinical management strategies and secured FDA authorization in 2020 for NSCLC with RET fusions and MTC harboring RET mutations, drawing from phase 1/2 investigations that documented objective response rates (ORRs) of 61–64% alongside intracranial efficacy [14, 15]. These compounds proficiently target both wild-type and mutated RET variants, while minimizing engagement with nontarget kinases and attenuating adverse reactions [16]. Nevertheless, drawbacks of synthetic TKI inhibitors—encompassing partial spectrum against resistance mutations, heterogeneous pharmacokinetic behaviors, and risks of protracted toxicities—have driven the broad implementation of natural substances as alternative or supplementary inhibitory modalities [17, 18].

Research indicates that natural inhibitors could more effectively stabilize ligand-RET complexes, mitigate off-target impacts, and improve therapeutic effectiveness across multiple cancer types, such as breast and colorectal carcinomas fueled by RET overexpression [19]. Natural substances inhibiting the receptor tyrosine kinase RET (Rearranged during Transfection) possess the capacity for diminished adverse effects and multitarget functionality relative to synthetic agents, as illustrated by contemporary computational analyses involving pharmacophore modeling, virtual screening, and molecular dynamics simulations that delineate scaffolds proficient in binding the RET kinase domain [20, 21]. In the context of RET specifically, pharmacoinformatics investigations have pinpointed auspicious scaffolds, including derivatives of propanoic, carboxylic, and hexanoic acids derived from repositories like ZINC, which display elevated binding free energies (BFE) toward wild-type and V804M/L mutant RET variants in comparison to vandetanib and selpercatinib [21-24]. These molecules establish robust hydrogen bonds with es-

sential residues like Ala807, Lys758, and Glu805, while sustaining structural stability throughout molecular dynamics simulations (mean RMSD of 1–3 Å over 150 ns) [21].

The adherence of natural inhibitors to Lipinski's rule of five, coupled with elevated gastrointestinal absorption, absence of liver toxicity, and advantageous ADMET characteristics, further indicates their viability as promising candidates for subsequent refinement [25]. Consequently, *in silico* drug discovery approaches have emerged as indispensable in this domain, leveraging high-resolution crystallographic data such as PDB entry 7JU6 (depicting the RET-selpercatinib complex at 2.06 Å resolution) encompassing the RET kinase domain (amino acids 705–1013) to inform inhibitor development [14]. This atomic model elucidates selpercatinib's interaction mechanism: it secures within the anterior pocket, extends around the gatekeeper wall into the posterior pocket, circumvents gatekeeper obstruction, yet remains susceptible to solvent front alterations [14, 26].

Leveraging the PDB entry 7JU6 facilitates the accurate detection and docking of natural inhibitors, allowing investigators to model binding dynamics for forecasting inhibitory efficacy and mitigating resistance challenges observed in established therapeutics like selpercatinib and pralsetinib employed in oncological interventions [13, 27]. Although RET-specific treatments have demonstrated clinical utility, debates persist concerning their sustained resistance profiles and nonspecific activities, underscoring the imperative for innovative inhibitors sourced from natural origins to augment therapeutic results in neoplasms harboring RET aberrations [28]. *In silico*-derived metrics frequently surpass those of benchmark inhibitors regarding binding affinity and conformational stability, notably in countering mutations that confer resistance. Moreover, assimilating these insights into comprehensive oncologic strategies may enhance patient prognoses, particularly in contexts enriched with RET activity, such as cerebral metastases or hormone therapy-resistant breast malignancies [10, 25]. Natural agents could exhibit synergistic effects alongside conventional TKIs, circumvent compensatory pathways, and augment pharmacokinetic properties [29]. Nonetheless, obstacles persist, including the substantiation of *in vitro* and *in vivo* potency as well as managing intricate molecular architectures during chemical synthesis [30]. Prospective avenues encompass the enhancement of pharmacophore frameworks via machine learning to broaden scaffold variety and the initiation of human studies to bridge computational discoveries with therapeutic implementation [31].

In essence, the in silico delineation of natural entities as RET antagonists, grounded in architectures like PDB 7JU6, constitutes an auspicious strategy for confronting RET-associated malignancies. The discernment of such antagonists through advanced computational workflows offers potential for devising more secure and resilient interventions within the dynamic realm of neoplastic signaling and pharmacoresistance.

Methods

Protein Preparation

The crystallographic three-dimensional architecture of the RET signaling cascade protein (PDB accession: 7JU6) was acquired from the Protein Data Bank (PDB) [32]. Structural preprocessing was performed utilizing the UCSF Chimera platform [33]. Extraneous moieties, including heteroatoms, hydration molecules, and ionic entities, were eliminated to generate an unadulterated protein conformation appropriate for molecular docking. Thereafter, energy minimization was executed to ameliorate any steric conflicts or conformational distortions. To evaluate the protein's pharmacological tractability, the optimized 3D configuration was inputted into the CavityPlus platform for cavity detection and evaluation.

Ligand Preparation

A compilation of 48 natural compound architectures was assembled from the ZINC12 repository [34]. Selection parameters included compliance with Lipinski's rule of five, a topological polar surface area (TPSA) below 70 $Å^2$, commercial procurability,

and provenance from the UEFS Natural Products repository. The chosen entities, acquired in SDF format, were processed utilizing PyRx software, encompassing geometric refinement and energy minimization.

Molecular Docking

In silico molecular docking analyses were executed utilizing the AutoDock Vina module integrated within the PyRx platform [35]. The preprocessed RET protein structure (7JU6) underwent docking procedures against the assemblage of 48 energy-minimized natural molecules. The docking search grid was configured with an exhaustiveness parameter of 8 and a central position at coordinates (x = -5.64, y = 0.51, z = 7.31). The grid box sizes were established at 55.51 Å (x), 38.82 Å (y), and 66.90 Å (z) to fully encapsulate the complete binding pocket.

Molecular Docking Results Analysis

This analysis was conducted utilizing the PLIP web-based platform [36].

Pharmacokinetic Property Prediction

The pharmacokinetic attributes of the leading compounds identified from the docking investigation were appraised employing the pkCSM online tool [37].

Results and Discussion

Assessment of the Druggability of RET

The structural druggability of RET kinase is marked by a distinctly outlined binding pocket, specified through key physicochemical and geometric features. This pocket presents a notable solvent-accessible surface area (SASA) of 895.50 $Å^2$ and a volume of 1592.00 $Å^3$, parameters that support the integration of various drug-like small molecules. In computational approaches such as molecular docking and virtual screening, the binding region is delineated by a grid box with dimensions of 22.5 Å × 14.5 Å × 17.5 Å, centered at coordinates (x = 13.75, y = 0.75, z = -7.75). These volumetric and configurational attributes align with those of a target exhibiting elevated druggability, facilitating robust interfaces for high-affinity ligand interactions and underpinning the therapeutic efficacy of targeted RET inhibitors (Table 1).

Molecular Docking Results

The four selected natural compounds—ZINC05202250, ZINC00338411, ZINC13374352, and ZINC13379108—show strong and stable interactions within the binding site of the RET kinase domain (PDB: 7JU6) based on molecular docking analyses, suggesting they could effectively inhibit this target.

These compounds displayed promising binding energies between -8.0 and -8.8 kcal/mol, reflecting favorable thermodynamics and substantial affinity for the RET active site. In particular, ZINC05202250 achieved the highest docking score of -8.8 kcal/mol. The root-mean-square deviation (RMSD) of 0.0 Å for the optimal pose of each compound indicates excellent conformational stability and precise fit with the binding pocket, as the docked configuration matches the lowest-energy state from the simulation.

Overall, these computational findings highlight the compounds as viable candidates for RET kinase inhibition, though additional advanced modeling and lab-based experiments are needed to confirm their effectiveness and interaction details (Table 2).

Table 1: Pocket of 7JU6

Surface Area (Å^2)	895.5
Volume (Å^3)	1592
Box Size (Å)	22.5 14.5 17.5
Box Center (Å)	13.75 0.75 -7.75
Residues	GLY-170-A,PHE-169-A,GLU-56-A,GLY-24-A,ILE-76-A, LYS-192-A,LYS-49-A,THR-17-A,LEU-157-A,SER-53-A, LEU-18-A,ASN-155-A,VAL-26-A,SER-55-A,ALA-52-A, GLY-102-A,GLU-22-A,GLU-20-A,ILE-156-A,ALA-152-A, LEU-48-A,SER-167-A,LEU-171-A,LYS-96-A,VAL-158-A, TYR-94-A,ILE-189-A,VAL-191-A,ASP-150-A,PRO-190-A, GLY-19-A,LEU-57-A,GLY-21-A,GLU-93-A,LEU-100-A, ILE-166-A,ASP-168-A,LEU-67-A,GLY-187-A,ALA-44-A, ARG-101-A,LEU-90-A,ALA-95-A,PRO-54-A,MET-47-A, VAL-92-A,TYR-97-A,SER-99-A,VAL-43-A,ARG-154-A, ARG-58-A,LYS-77-A,ASP-59-A,ARG-188-A,LYS-46-A, GLU-63-A,LYS-25-A,LYS-165-A,PHE-23-A,LEU-61-A, GLY-98-A,TRP-193-A,VAL-27-A,VAL-45-A,ALA-153-A,LEU-60-A

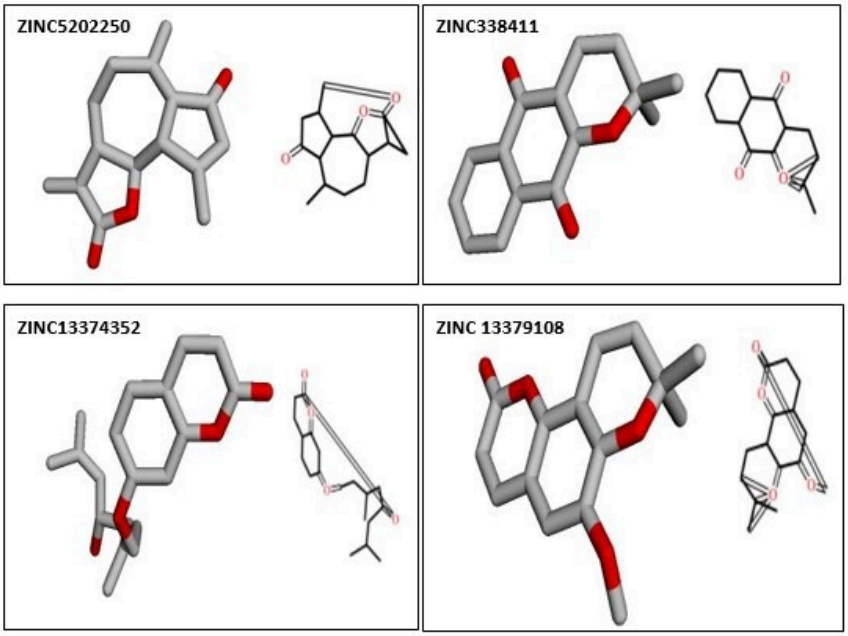

Figure 1: 2D, 3D Structure of Selected Natural Compounds

Table2: High Affinity Natural Compounds within the RET

Ligand	Binding Affinity	RMSD lower bound
7ju6_ZINC69482416_uff_E=541.34	-10.1	0
7ju6_ZINC00006256_uff_E=357.76	-9.5	0
7ju6_ZINC01846592_uff_E=456.68	-9.5	0
7ju6_ZINC00306698_uff_E=451.82	-9.4	0
7ju6_ZINC00306698_uff_E=454.08	-9.4	0
7ju6_ZINC05202250_uff_E=421.30	-8.8	0

7ju6_ZINC13374022_uff_E=388.69	-8.6	0
7ju6_ZINC00338411_uff_E=193.02	-8.6	0
7ju6_ZINC01611275_uff_E=195.76	-8.6	0
7ju6_ZINC00895662_uff_E=383.58	-8.5	0
7ju6_ZINC28536305_uff_E=548.14	-8.3	0
7ju6_ZINC02563652_uff_E=391.73	-8.2	0
7ju6_ZINC28536305_uff_E=541.52	-8.1	0
7ju6_ZINC13374352_uff_E=209.15	-8	0
7ju6_ZINC13379108_uff_E=221.03	-8	0

Furthermore, the configurations of hydrogen bonds and ionic linkages delineate the selectivity profiles of individual compounds. Both ZINC05202250 and ZINC13379108 leverage hydrogen bonding, with the former connecting to LYS46A and ASP168A, and the latter forging a broader linkage array with LEU18A, GLU93A, and ALA95A. Strikingly, ZINC13374352 establishes a solitary yet vital salt bridge with LYS46A, a residue that consistently features in both hydrophobic and polar dynamics across the examined set. This duality emphasizes LYS46A's multifunctional significance as a primary docking anchor, presumably vital for precise inhibitor alignment within the ATP-competitive domain. In contrast, the omission of hydrogen bonds in ZINC00338411's profile indicates that its stabilization hinges primarily on pronounced hydrophobic congruence. Overall, these interaction blueprints demonstrate that while durable hydrophobic engagements with a conserved residue cohort deliver the principal energetic foundation, the heterogeneity in hydrogen bonding and salt bridge architectures imparts distinctive docking imprints and likely influences the modulatory efficacy of each ligand (Fig. 2.A-D).

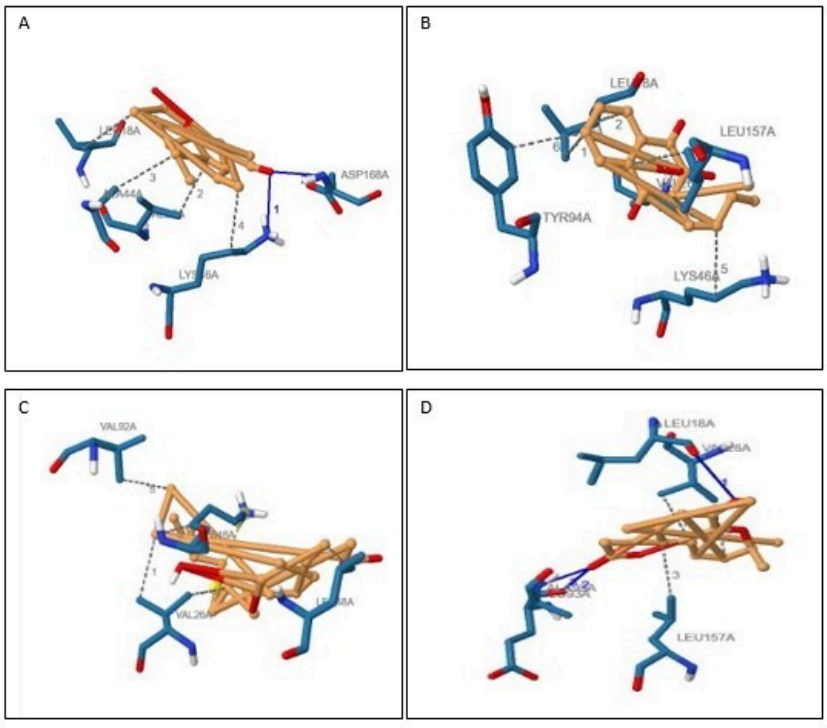

Figure 2: ZINC 5202250 and 7JU6 Interaction (A); ZINC338411 and 7JU6 Interaction (B); ZINC13374352 and 7JU6 Interaction (C); ZINC 13379108 and 7ju6 Interaction (D)

Table 3: Molecular Interaction Profiles Of High Affinity Natural Compounds within the RET Active Site

Receptor-Ligand complex	Hydrophobic interaction	Hydrogen interaction	Salt bridge
7ju6_ZINC05202250	LEU18A,VAL26A,ALA44A,LYS46A	LYS46A,ASP168A	
7ju6_ZINC00338411	LEU18A,VAL26A,LYS46A,TYR94A,LEU157A		
7ju6_ZINC13374352	VAL26A,LYS46A,LEU48A,VAL92A		LYS46A
7ju6_ZINC13379108	VAL26A,LEU157A	LEU18A,GLU93A,ALA95A	

Pharmacokinitics Properties

The pharmacokinetic absorption characteristics of compounds L1 to L4 were assessed via computational predictive frameworks. These analyses reveal marked differences in their biopharmaceutical viability. Specifically, L1, L2, and L4 display advantageous and comparable absorption attributes, with forecasted human intestinal absorption rates surpassing 97%. This is corroborated by elevated Caco-2 cell permeability metrics, each exceeding the 0.90 benchmark indicative of superior permeability, implying effective passage through the gut epithelium. Although these compounds show modest aqueous solubility, a typical feature among pharmacologically relevant entities, their robust permeability suggests that solubility does not impede absorption, positioning them within Biopharmaceutics Classification System (BCS) Class II. Importantly, L1, L2, and L4 are not anticipated to act as substrates or inhibitors of P-glycoprotein (P-gp), thereby minimizing risks of efflux-mediated absorption hindrance or P-gp-related pharmacokinetic interactions.

Conversely, L3 exhibits a multifaceted profile with potential drawbacks. Despite a commendable predicted intestinal absorption of 95.2% and strong Caco-2 permeability, it carries notable vulnerabilities. L3 is projected to function as both a P-gp substrate and a Type I inhibitor, heightening the likelihood of adverse drug interactions; this could diminish its own systemic exposure via efflux while impeding the elimination of concomitant P-gp-dependent medications, risking elevated and potentially harmful blood levels. Additionally, L3 demonstrates the lowest water solubility in the cohort, which may further complicate dissolution and uptake. Thus, whereas L1, L2, and L4 stand out as viable leads with unencumbered absorption and minimal interaction liabilities, advancing L3 demands rigorous evaluation owing to its elevated interaction risks and suboptimal solubility.

Based on the provided data and referenced interpretation guidelines, the distribution profiles of compounds L1 through L4 reveal significant differences in their potential to distribute within the body, particularly in their tissue penetration and central nervous system (CNS) exposure.

The predicted Volume of Distribution at steady state (VDss) for all four compounds is low, with log values substantially below the threshold of -0.15. This indicates that these molecules are predominantly confined to the systemic circulation rather than extensively distributing into peripheral tissues. Notably, L3 exhibits a relatively higher VDss compared to the others, particularly L4 which shows the most restricted distribution.

Examination of the unbound fraction in human plasma (Fu) reveals that each of the compounds displays substantial plasma protein binding. Notably, L3 exhibits the most pronounced binding affinity, with merely 9.6% remaining unbound and thus available for pharmacological action. In comparison, L1, L2, and L4 present elevated unbound fractions of 36.99%, 23.8%, and 24.8%, respectively, implying a larger bioactive portion capable of engaging with physiological targets.

With respect to central nervous system (CNS) accessibility, the logarithm of the blood-brain barrier (logBB) permeability indicates that L2 demonstrates intermediate penetrative capacity at -0.648, a value that, although subzero, surpasses those of its counterparts and nears the criterion for meaningful CNS engagement. Conversely, L1, L3, and L4 are forecasted to exhibit limit-

ed cerebral distribution, with L3 showing the greatest impediment. This evaluation is corroborated by the CNS permeability metric (logPS), which provides a kinetic perspective on brain influx. All compounds register logPS values under -2, signifying restricted CNS entry. Nonetheless, L2 manifests the most favorable permeation potential within this cohort, though still beneath the -2 benchmark, whereas L4 appears the least permeable.

Utilizing the furnished dataset and established pharmacokinetic tenets, the biotransformation characteristics of compounds L1 to L4 were scrutinized, emphasizing their engagements with principal cytochrome P450 (CYP) isozymes. The outcomes delineate a collective metabolic route for the quartet, yet underscore pivotal variances in their propensity for pharmacodynamic interplays.

A consistent observation among the four entities is their forecasted designation as substrates for the CYP3A4 variant, whereas none are projected to undergo catalysis via CYP2D6. This homogeneous vulnerability to CYP3A4-catalyzed biotransformation implies that the disposition kinetics of these agents, notably their elimination velocities, may be profoundly influenced by concomitants with robust CYP3A4 suppressors (e.g., ketoconazole) or activators (e.g., rifampin), precipitating plausible escalations or diminutions in their circulatory concentrations, accordingly.

In terms of their suppressive capabilities, the entirety of compounds (L1–L4) are anticipated to attenuate the CYP1A2 isoform. This uniformity engenders a persistent hazard for drug-drug interferences with co-prescribed agents reliant on CYP1A2 for clearance, such as clozapine or theophylline, conceivably culminating in augmented serum titers of these pharmaceuticals. Of greater import, the suppressive spectra bifurcate for additional CYP variants. Entities L1 and L2 manifest a comparatively unencumbered spectrum, evincing no foreseen attenuation of CYP2C19, CYP2C9, CYP2D6, or CYP3A4. Conversely, L3 evinces the paramount interplay jeopardy, with anticipated suppression of both CYP2C19 and CYP2C9 alongside CYP1A2. Compound L4 evinces a transitional spectrum, restraining CYP2C19 yet sparing CYP2C9. An auspicious revelation for the cohort is the absence of restraint against CYP2D6 and CYP3A4, representing two paramount isoforms pivotal to pharmaceutical catabolism.

The elimination characteristics of compounds L1 to L4, assessed through *in silico* estimates of total clearance (log(CLtot)) and affinity for the renal organic cation transporter 2 (OCT2), exhibit heterogeneous kinetic patterns. Computational analysis of log(CLtot) highlights considerable heterogeneity within the series, with L3 forecasted to display the most rapid clearance, nearing the model's maximum, implying swift bodily removal. Conversely, L2 manifests markedly reduced clearance, suggestive of extended circulatory persistence. L1 and L4 present comparable moderate clearance metrics, indicative of balanced elimination rates.

Uniformly across the quartet, predictions indicate non-substrate status for OCT2, implying that renal disposition and excretion bypass this facilitative mechanism. This diminishes prospects for drug-drug interactions with OCT2 modulators and insulates renal clearance from genetic variants or competitive dynamics at this transporter.

Drawing from computational simulations and toxicological standards, the risk assessments for L1 through L4 encompass multiple parameters. Notably, all are deemed non-mutagenic per AMES projections, connoting minimal genotoxic or carcinogenic hazards. Additionally, absence of forecasted hERG blockade (types I or II) portends reduced arrhythmogenic liabilities, including QT prolongation. The series universally lacks anticipated dermal irritancy.

Evaluations of short- and long-term mammalian hazards delineate varied signatures. Oral rat LD50 estimates denote intermediate acute lethality for the cohort, with L3 evincing the greatest intensity. In chronic paradigms, LOAEL metrics position L2 with the broadest therapeutic window (elevated LOAEL), whereas L3 registers the narrowest adversity onset. Hepatotoxicity emerges as a key discriminator, with solely L2 implicated in potential hepatic impairment. Human maximum tolerated dose extrapolations reinforce these disparities, favoring L2 for superior exposure tolerance and constraining L4 to the lowest thresh-

old.

Assessment of ecotoxicological endpoints shows varying results. In the predicted T. Pyriformis toxicity, compounds L3 and L4 exhibit toxicity, with pIGC50 values exceeding the -0.5 log μg/L threshold, whereas L1 and L2 are below this level of concern. In the predicted Minnow toxicity, all compounds have log LC50 values greater than the -0.3 threshold, indicating low acute toxicity to fish; however, L1 and L2 demonstrate the highest potential for aquatic toxicity within this series.

The integrated *in silico* ADMET profiling of the natural compounds L1-L4 reveals critical insights into their potential as viable drug candidates for targeting the RET signaling pathway in cancer. The analysis identifies a clear divergence in candidate suitability, with compounds L1, L2, and L4 exhibiting particularly promising pharmacokinetic profiles. These molecules are predicted to have high intestinal absorption, aligning with Biopharmaceutics Classification System (BCS) Class II, and present a low risk of P-glycoprotein-mediated drug interactions, a crucial advantage for maintaining consistent oral bioavailability. Their uniformly low potential for CNS penetration suggests a peripheral site of action, which could be beneficial for minimizing neurotoxic side effects in the treatment of peripheral cancers. Furthermore, the clean cardiotoxicity (hERG negative) and genotoxicity (AMES negative) profiles across the series substantially de-risk these candidates from critical safety failures in early development, establishing a strong foundation for their progression as RET inhibitors.

When prioritizing among the lead candidates, L1 and L4 emerge as the most balanced, possessing favorable absorption, a manageable metabolic profile characterized by selective CYP inhibition, and moderate clearance. In contrast, L2's predicted hepatotoxicity represents a significant liability that necessitates caution, despite its otherwise attractive profile. Compound L3, while pharmacologically active, is burdened by a high propensity for drug-drug interactions, acting as both a substrate and inhibitor of P-glycoprotein and a broad inhibitor of multiple CYP450 enzymes, alongside a poorer solubility and higher predicted toxicity. This comprehensive multi-parametric *in silico* assessment effectively triages the compound series, underscoring that while L1 and L4 warrant priority for further experimental validation in RET-driven models, L2 and L3 present higher risks that may preclude their development without significant structural optimization (Table 4).

Table 4: Pharmacokinitics Properties (ZINC05202250 (L1), ZINC00338411 (L2), ZINC13374352 (L3), ZINC13379108 (L4)

Property	Model Name	Value	Unit
Absorption	Water solubility	L1(-3.103),L2(-3.425),L3(-4.747),L4(-3.233)	Numeric (log mol/L)
Absorption	Caco2 permeability	L1(1.286),L2(1.334),L3(1.373),L4(1.355)	Numeric (log Papp in 10^{-6} cm/s)
Absorption	Intestinal absorption (human)	L1(98.607),L2(97.665),L3(95.247),L4(97.196)	Numeric (% Absorbed)
Absorption	Skin Permeability	L1(-3.031),L2(-2.677),L3(-2.615),L4(-2.5)	Numeric (log Kp)
Absorption	P-glycoprotein substrate	L1(No),L2(No),L3(Yes),L4(No)	Categorical (Yes/No)
Absorption	P-glycoprotein I inhibitor	L1(No),L2(No),L3(Yes),L4(No)	Categorical (Yes/No)
Absorption	P-glycoprotein II inhibitor	L1(No),L2(No),L3(No),L4(No)	Categorical (Yes/No)
Distribution	VDss (human)	L1(0.163),L2(0.117),L3(0.327),L4(0.02)	Numeric (log L/kg)
Distribution	Fraction unbound (human)	L1(0.3699),L2(0.238),L3(0.096),L4(0.248)	Numeric (Fu)
Distribution	BBB permeability	L1(0.085),L2(0.648),L3(0.026),L4(0.201)	Numeric (log BB)

Distribution	CNS permeability	L1(-2.534),L2(-2.38),L3(-2.243),L4(-2.605)	Numeric (log PS)
Metabolism	CYP2D6 substrate	L1(No),L2(No),L3(No),L4(No)	Categorical (Yes/No)
Metabolism	CYP3A4 substrate	L1(Yes),L2(Yes),L3(Yes),L4(Yes)	Categorical (Yes/No)
Metabolism	CYP1A2 inhibitior	L1(Yes),L2(Yes),L3(Yes),L4(Yes)	Categorical (Yes/No)
Metabolism	CYP2C19 inhibitior	L1(No),L2(No),L3(Yes),L4(Yes)	Categorical (Yes/No)
Metabolism	CYP2C9 inhibitior	L1(No),L2(No),L3(Yes),L4(No)	Categorical (Yes/No)
Metabolism	CYP2D6 inhibitior	L1(No),L2(No),L3(No),L4(No)	Categorical (Yes/No)
Metabolism	CYP3A4 inhibitior	L1(No),L2(No),L3(No),L4(No)	Categorical (Yes/No)
Excretion	Total Clearance	L1(0.629),L2(0.077),L3(0.999),L4(0.603)	Numeric (log ml/min/kg)
Excretion	Renal OCT2 substrate	L1(No),L2(No),L3(No),L4(No)	Categorical (Yes/No)
Toxicity	AMES toxicity	L1(No9,L2(No),L3(),L3(No),L4(No)	Categorical (Yes/No)
Toxicity	Max. tolerated dose (human)	L(0.08),L(0.763),L3(0.448),L4(-0.054)	Numeric (log mg/kg/day)
Toxicity	hERG I inhibitor	L1(No),L2(No),L3(No),L4(No)	Categorical (Yes/No)
Toxicity	hERG II inhibitor	L1(No),L2(No),L3(No),L4(No)	Categorical (Yes/No)
Toxicity	Oral Rat Acute Toxicity (LD50)	L1(1.847),L2(2.126),L3(2.333),L4(2.195)	Numeric (mol/kg)
Toxicity	Oral Rat Chronic Toxicity (LOAEL)	L1(1.661),L2(2.047),L3(1.453),L4(1.614)	Numeric (log mg/kg_bw/day)
Toxicity	Hepatotoxicity	L1(No),L2(Yes),L3(No),L4(No)	Categorical (Yes/No)
Toxicity	Skin Sensitisation	L1(No),L2(No),L3(No),L4(No)	Categorical (Yes/No)
Toxicity	T.Pyriformis toxicity	L1(0.74),L2(0.929),L3(1.511),L4(1.228)	Numeric (log ug/L)
Toxicity	Minnow toxicity	L1(1.41),L2(1.01),L3(0.367),L4(0.711)	Numeric (log mM)

Conclusion

This integrated *in silico* study successfully identifies four natural compounds, ZINC05202250, ZINC00338411, ZINC13374352, and ZINC13379108, as highly promising candidates for inhibiting the RET signaling pathway in cancer. The multi-stage computational workflow, combining structure-based virtual screening, molecular docking, and comprehensive ADMET profiling, demonstrates that these ligands form thermodynamically stable complexes with the RET kinase domain, evidenced by strong

binding energies ranging from -8.0 to -8.8 kcal/mol. Critically, the compounds are characterized by favorable predicted pharmacokinetic properties, including high intestinal absorption and a low potential for cardiotoxicity and genotoxicity. Furthermore, the distinct interaction profiles, featuring key hydrophobic contacts with residues such as VAL26A and LYS46A, complemented by specific hydrogen bonds and salt bridges, suggest a robust mechanism of action within the well-defined druggable pocket of RET.

While compounds ZINC05202250 and ZINC13379108 emerge as the most balanced leads due to their optimal binding affinity, cleaner metabolic profiles, and lower predicted toxicological liabilities, this research collectively underscores the viability of targeting RET with natural product-derived inhibitors. The findings provide a strong and rational foundation for subsequent experimental validation, recommending these candidates for further investigation in *in vitro* enzymatic assays and *in vivo* models of RET-driven cancers to confirm their therapeutic potential and refine their chemical scaffolds for future drug development.

References

1. Singh A, Roghini S (2023) Cancer: Unraveling the complexities of uncontrolled growth and metastasis. PEXACY International Journal of Pharmaceutical Science, 2: 59-73.

2. Ruby M (2025) An introduction to receptor tyrosine kinases: Signal transduction and cancer progression. In: Receptor Tyrosine Kinases in Cancer. Springer, 1-24.

3. Cheng J (2025) Investigating the roles of truncated kinases in oncogenic signal rewiring. University of Toronto, Canada.

4. Hong C (2023) Analysis of whole-genome sequencing data from the ICGC-PanCancer project.

5. Desilets A (2023) RET-altered cancers: A tumor-agnostic review of biology, diagnosis and targeted therapy activity. Cancers, 15: 4146.

6. Chen Y (2024) Identifying predictive biomarkers and novel drug targets in small cell lung cancer via multi-omics analysis. University of Manchester, United Kingdom.

7. Regua AT, Najjar M, Lo HW (2022) RET signaling pathway and RET inhibitors in human cancer. Frontiers in Oncology, 12: 932353.

8. Sahakian N, Castinetti F, Romanet P (2023) Molecular basis and natural history of medullary thyroid cancer: It is (almost) all in the RET. Cancers, 15: 4865.

9. Liu Y (2024) Abstracts of the 36th European Congress of Pathology. Virchows Archiv, 485: S1-S546.

10. Pecar G (2023) RET signaling in breast cancer therapeutic resistance and metastasis. Breast Cancer Research, 25: 26.

11. Spitaleri G (2024) Non-small-cell lung cancers harboring RET gene fusion: From discovery to selective RET inhibitors. Cancers, 16: 2877.

12. Yayan J (2024) Adhesion, metastasis, and inhibition of cancer cells: A comprehensive review. Molecular Biology Reports. 51: 165.

13. Wang ZX (2024) Unraveling the promise of RET inhibitors in precision cancer therapy. Journal of Medicinal Chemistry. 67: 4346-75.

14. Subbiah V (2021) Structural basis of acquired resistance to selpercatinib and pralsetinib mediated by non-gatekeeper RET mutations. Annals of Oncology. 32:261-8.

15. Subbiah V (2018) Selective RET kinase inhibition for patients with RET-altered cancers. Annals of Oncology. 29: 1869-76.

16. Thein KZ (2021) Precision therapy for RET-altered cancers with RET inhibitors. Trends in Cancer. 7: 1074-88.

17. Alrumaihi F (2025) Role of plant-derived natural products in regulation of the tyrosine kinase pathway in lung cancer. Current Issues in Molecular Biology. 47: 498.

18. Attili I (2023) New generations of tyrosine kinase inhibitors in oncogene-addicted NSCLC. Cancers. 15: 5079.

19. Addeo A (2023) RET aberrant cancers and RET inhibitor therapies: Current state and future perspectives. Pharmacology and Therapeutics. 242: 108344.

20. Mohamed AR, El Kerdawy AM (2022) RTK, PI3K, B-Raf and CDK targeting strategies in medicinal chemistry. Chemistry and Biodiversity.19: e202200328.

21. Parate S (2022) Natural compounds targeting oncogenic RET tyrosine kinase using pharmacoinformatics. RSC Advances. 12: 1194-207.

22. Durdagi S (2024) Structure-based pharmacophore and QSAR models for resistance-free RET inhibitors. Biophysical Journal. 123: 473a.

23. Parate S (2022) Dual inhibitors of mTOR and RET kinase from natural products. Journal of Molecular Liquids. 350: 118562.

24. Talukder MEK (2024) Cheminformatics-based identification of phosphorylated RET inhibitors. Frontiers in Chemistry. 12: 1407331.

25. S AS (2024) Computational identification of potential RET inhibitors for targeted lung cancer therapy.

26. Raj PE, Bhaskar R, Anne S (2024) Selpercatinib: A narrative drug review. Cancer Research, Statistics, and Treatment. 7: 82-90.

27. Zhong J (2025) Discovery of APS03118, a potent next-generation selective RET inhibitor. Journal of Medicinal Chemistry.

28. Subbiah V (2024) Adaptive off-target resistance mechanisms to selective RET inhibition. NPJ Precision Oncology. 8: 62.

29. Chen JW, Chen S, Chen GQ (2025) Synergizing tyrosine kinase inhibitors with natural products in liver cancer. Discover Molecules. 2: 1-11.

30. Mittal R (2025) Exploring the potential of computer simulation models in drug testing and biomedical research. Frontiers in Pharmacology. 16: 44907.

31. Gangwal A, Lavecchia A (2025) Artificial intelligence in natural product drug discovery. Journal of Medicinal Chemistry. 68: 3948-69.

32. Berman HM, Westbrook J, Feng Z, Gilliland G, Bhat TN, et al. (2000) The Protein Data Bank. Nucleic Acids Research. 28: 235-42.

33. Pettersen EF (2004) UCSF Chimera: A visualization system for exploratory research. Journal of Computational Chemistry 25: 1605-12.

34. Sterling T, Irwin JJ (2015) ZINC: Ligand discovery for everyone. Journal of Chemical Information and Modeling.

35. Dallakyan S, Olson AJ (2014) Small-molecule library screening by docking with PyRx. In: Chemical Biology: Methods and Protocols. Springer. 243-50.

36. Schake B, Bolz S (2025) PLIP 2025: Introducing protein–protein interactions to the protein–ligand interaction profiler.

37. Pires DE, Blundell TL, Ascher DB (2015) pkCSM: Predicting pharmacokinetic and toxicity properties. Journal of Medicinal Chemistry. 58: 4066-72.